ELSEVIER

Journal of Magnetism and Magnetic Materials 233 (2001) 195–204

Journal of magnetism and magnetic materials

www.elsevier.com/locate/jmmm

Preparation and magnetic properties of Fe–Ag granular alloy

Suwen Liu[a], Lunxiang Yin[a], Yuri Koltypin[a], Aharon Gedanken[a,*], Xiaonong Xu[b], Yosi Yeshurun[b], Israel Felner[c], Gad Gorodetsky[d]

[a] *Department of Chemistry, Bar-Ilan University, Ramat-Gan 52900, Israel*
[b] *Department of Physics, Bar-Ilan University, Ramat-Gan 52900, Israel*
[c] *Racah Institute of Physics, Hebrew University, Jerusalem, Israel*
[d] *Department of Physics, Ben-Gurion University, Beer Sheba, Israel*

Received 16 November 2000

Abstract

An aqueous solution of $AgNO_3$ in the presence of ammonia and $Fe(CO)_5$ is sonicated under a H_2/Ar mixture, yielding a nanostructured homogeneous phase of Ag/Fe_2O_3. This composite material is further reduced at 300°C under hydrogen to produce the nanophased Fe/Ag solid mixture. The as-prepared material, as well as the reduced mixture, is analyzed by various conventional methods. Magnetization loops, ESR, Mössbauer, and magnetoresistance measurements are also conducted to determine the magnetic properties of the products.

PACS: 75.50.K; 81.05.Y

Keywords: Sonochemistry; Nanotechnology; Alloys; Magnetic materials

1. Introduction

The synthesis of unusual and nanometer-scale materials has been the focus of intense study in materials science and solid-state chemistry [1,2]. Nanosized particles of noble metals have attracted considerable interest in various fields of chemistry because of their conspicuous physiochemical catalytic properties and their potential applications in microelectronics, optical, electronic, and magnetic devices [3–6]. Much attention have been paid to granular iron solids because of their interesting physical properties and their applications in magnetic recording, optical devices, and sensors [7–9].

Nanocrystalline (NC) Fe particles containing a single magnetic domain exhibit magnetic properties that are strikingly different from those of bulk Fe. New applications may exist for materials that combine that high magnetization and coercivity of single domain Fe particles together with a highly conducting matrix. Fe can form alloys or solid solutions with almost any metal, while there are a few metallic elements with which Fe is immiscible. Ag is one such example for the latter. However, in recent years, it has been shown that metastable and homogeneous alloys of Fe–Ag system can be formed by using special techniques, such as

*Corresponding author. Fax: +972-3-535-1250.
E-mail addresses: gedanken@mail.biu.ac.il (A. Gedanken), suwen@cat.hocudai.ac.jp (S. Liu).

0304-8853/01/$ - see front matter
PII: S0304-8853(01)00169-X

thermal evaporation [10,11], liquid quenching [12], ion implantation [13], sputtering [14–18], mechanical alloying [19,20], and the gas condensation method [21]. Fe/Ag alloy, however, is metastable, and upon recrystallization at elevated temperatures, a transformation into separated phases of BCC Fe and FCC Ag occurs.

Sumiyama and co-workers [22] have reported that Fe–Ag granular alloy prepared by an ion cluster beam exhibit the largest magnetoresistance (MR) in the as-deposited sample, where the small Fe clusters were dispersed in the Ag matrix. The maximum MR can also be obtained when nanometric Fe clusters are dispersed in conductive silver matrices indirectly by the annealing of homogeneous deposited alloys. Since giant magnetoresistance (GMR) originates from the difference between conduction electron scattering in the demagnetized and magnetized states, the magnetic atoms in clusters and at the interfaces between the magnetic and nonmagnetic regions play an important role [23].

The sonochemical method is a relatively new technique for the preparation of nanosized amorphous powders of Fe, Co, and their alloys [24–29]. The current paper describes the sonochemistry-reduction synthesis and characterization of nanosized granular Fe/Ag alloy. The Fe/Ag alloy cannot be obtained directly in large quantities by the sonochemical method. The NC (nanocrystalline) Fe/Ag is, however, fabricated by annealing the sonochemically as-prepared Ag/Fe_2O_3 product under H_2 at 300°C.

2. Experimental

0.15 g (0.30 g, 0.25 g) $AgNO_3$ was dissolved in 10 ml water, and then 0.5 ml $NH_3 \cdot H_2O$ was added into the solution. This solution and 5 ml (0.5 ml, 0.25 ml) of pure $Fe(CO)_5$ were mixed in a 50 ml sonication cell, by adding water until the value of the mixture reached 50 ml. After removal of the O_2 by bubbling Ar for 1 h, the mixture was irradiated with a high intensity ultrasonic horn under 1 atmosphere Ar/H_2 at 0°C for 1.5 h. The H_2 is the reducing agent in the gaseous mixture. The product was then washed with dry pentane and pure water in an inert glove box. This product is identified as a homogeneous mixture of Fe_2O_3 and Ag. The Ag/Fe granular alloy is further fabricated from this homogeneous mixture by annealing the as-prepared Ag/Fe_2O_3 product under pure H_2 at 300°C for 1.5 h. The composition of the solid product and especially the ratio of Fe/Ag was determined by EDAX. Energy dispersive X-ray (EDX) on a JEOL JSM-840 electron microscope was used to carry out elemental analyses. An additional and more accurate measurement to determine the ratios of silver and iron was carried out using a traditional chemical method. The differential scanning calorimetric (DSC) spectrum was recorded using a Mettler Toledo (DSC 25) Instrument. The heating rate was 10°C/min. Magnetic force measurements were carried out on a Mettler TGA4000 with a small permanent magnet. The X-ray diffraction patterns were recorded by employing a Rigaku X-ray diffractometer (Model-2028, Cu K_α). Samples were also analyzed on a JEOL JEM-1220 transmission electron microscope (TEM).

The Mössbauer spectroscopy (MS) studies were carried out at 85 and 300 K, using a conventional constant acceleration spectrometer. The ^{57}Fe MS was measured with a 50 mCi $^{57}Co:Rh$ source, and the spectra were least square fitted, with one or two sub-spectra. The isomer shift (IS) values are relative to Fe metal at 300 K.

To enable the electric resistivity and magnetoresistance measurements of the Ag_xFe_{1-x} samples, the powders were first pressed (at a pressure of about 5 kbar) to form solid pellets and then electrically wired for customary four point measurements.

3. Results and discussion

3.1. XRD, EDX

Elemental analysis by EDX shows that the resulting black powder contains the elements Fe, Ag, and O (Fig. 1). The atomic ratio of Ag : Fe is about 1 : 1. The presence of oxygen leads, perhaps, to a conclusion that the product in this case is composed of Ag/Fe_2O_3. However, the XRD

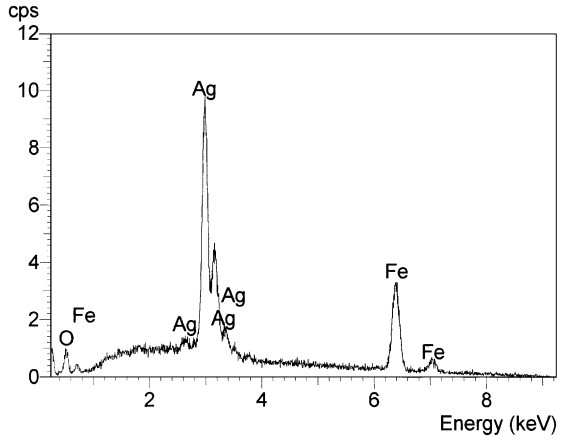

Fig. 1. The results of elemental analysis by EDX.

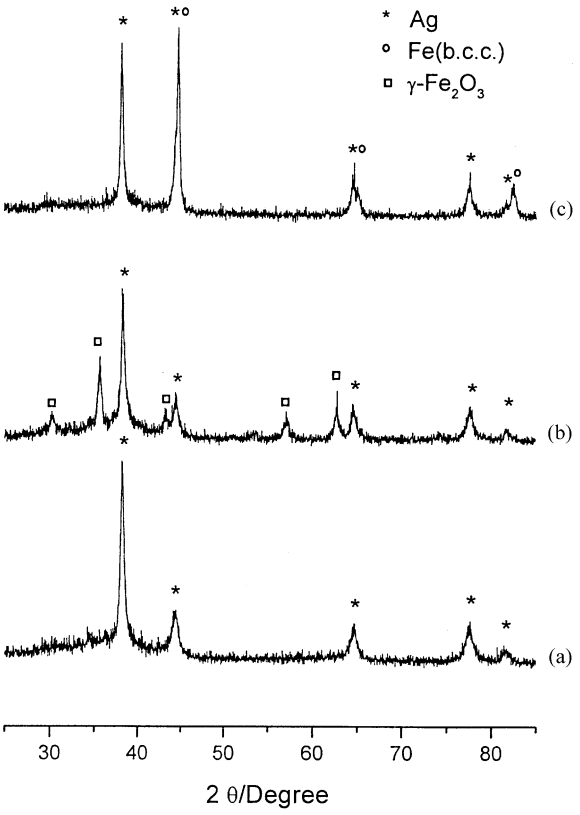

Fig. 2. XRD patterns of samples: (a) the as-prepared sample; (b) the as-prepared sample, annealed under Ar at 350°C for 1.5 h. (c) the as-prepared sample, annealed under H_2 at 300°C for 1.5 h.

patterns of the as-prepared sample shows only the Ag peaks. Neither Fe nor FeO_x peaks are detected in the XRD spectrum (Fig. 2a). After annealing the as-prepared product under Ar at 350°C for 1.5 h, peaks of Fe_2O_3 appeared (Fig. 2b). This result indicates that the as-prepared product is a mixture of amorphous Fe_2O_3 and nano-sized silver particles. After annealing under pure H_2 at 300°C for 1.5 h, the XRD patterns show only the peaks of the iron and silver (Fig. 2c). It is shown that the iron in the nanocrystalline (NC) Fe/Ag is BCC structure (JCPDS 6-696), while the silver is FCC structure (JCPDS 4-783). Fig. 3 shows the XRD patterns of NC Fe/Ag systems ($Fe_{70}Ag_{30}$, $Fe_{50}Ag_{50}$ and $Fe_{30}Ag_{70}$, determined by EDAX). The diffraction patterns reveal that the relative height of the peaks at around $2\theta = 44^\circ$ are strongly dependent on the Fe : Ag ratio. Though the BCC Fe spectral lines overlap with some of the

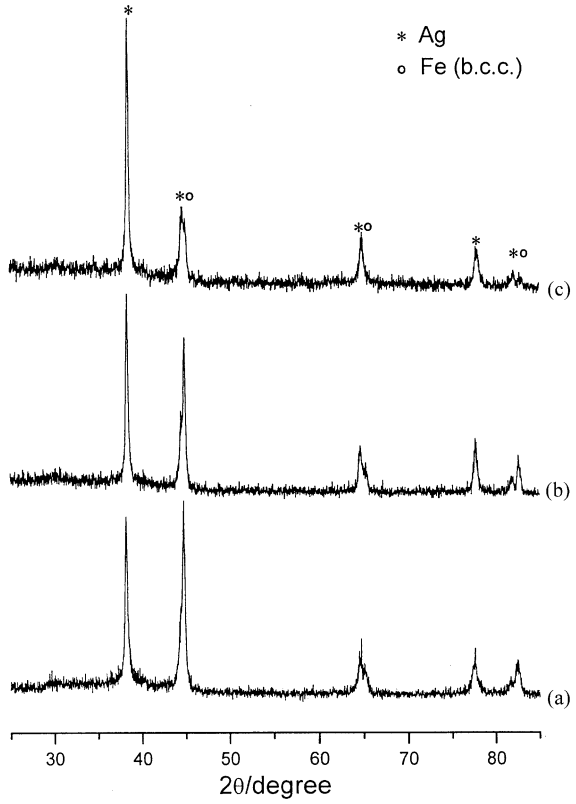

Fig. 3. XRD patterns of NC Fe/Ag systems: (a) $Fe_{70}Ag_{30}$; (b) $Fe_{50}Ag_{50}$; (c) $Fe_{30}Ag_{70}$.

Ag lines, separated peaks for Ag and Fe can still be detected, especially at high 2Θ angle. After annealing under pure H_2 at 300°C for 1.5 h, the average size of the silver particles increases up to 34 nm from 19 nm (deduced by employing the Debye–Scherrer formula). These results indicate that the sample is a mixture of NC Ag and Fe.

3.2. DSC and TGA

The DSC curves of the as-prepared sample (Fig. 4) show that there are two exothermal peaks at around 200°C and 310°C, respectively. We attribute these peaks to the crystallization of amorphous products in the sample. This interpretation is based on the fact that when the sample is cooled down (after it has been heated) to room temperature and the DSC is remeasured, the exothermic peaks are not observed. From these results we conclude that the as-prepared product is a mixture of amorphous materials (iron oxide and partial silver) and nanostructured silver particles. The crystallization of the Fe_2O_3 is known to occur around 300°C, therefore we attribute the 200°C exothermic peak to the crystallization of silver.

Figs. 5(a, b and c) show the results of a magnetic force measurement, obtained with a thermogravimetric balance, on the samples of NC Fe/Ag. The apparent drop in mass detected around 570°C is attributed to the Curie point (T_c) of NC Fe in the silver matrix. For the three samples of different ratios of Fe and Ag, the T_c is almost same. On the other hand, in the TG curve of a NC Fe/Ag (50 : 50), in the absence of a magnetic field, there is no such change (Fig. 5d), and a smooth line is detected.

3.3. SEM and TEM

Fig. 6 shows a typical SEM image of the as-prepared sample (Fe : Ag = 70 : 30). It depicts a homogenous mixture of amorphous products and NC Ag. All of the particles are aggregated in a spongelike form, and therefore, it is difficult to determine accurately the individual particle sizes. (Figs. 7a, b, and c show the TEM images of the corresponding samples appearing in Figs. 2a, b, and c, respectively). The as-prepared sample in

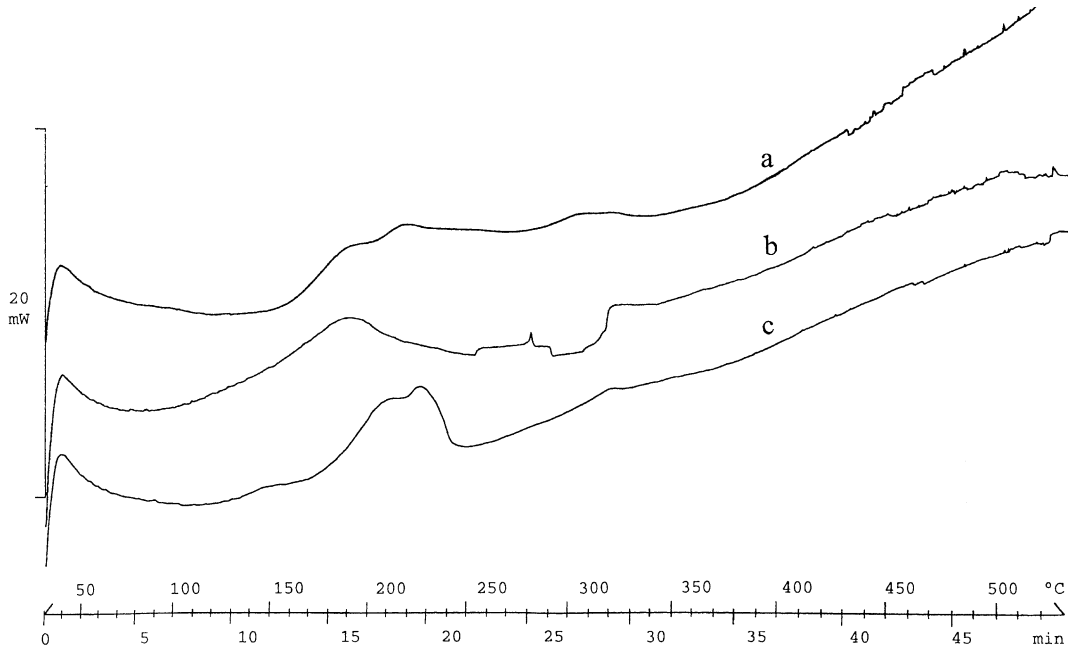

Fig. 4. The DSC curves of the as-prepared samples: (a) $Fe_{70}Ag_{30}$; (b) $Fe_{50}Ag_{50}$; (c) $Fe_{30}Ag_{70}$.

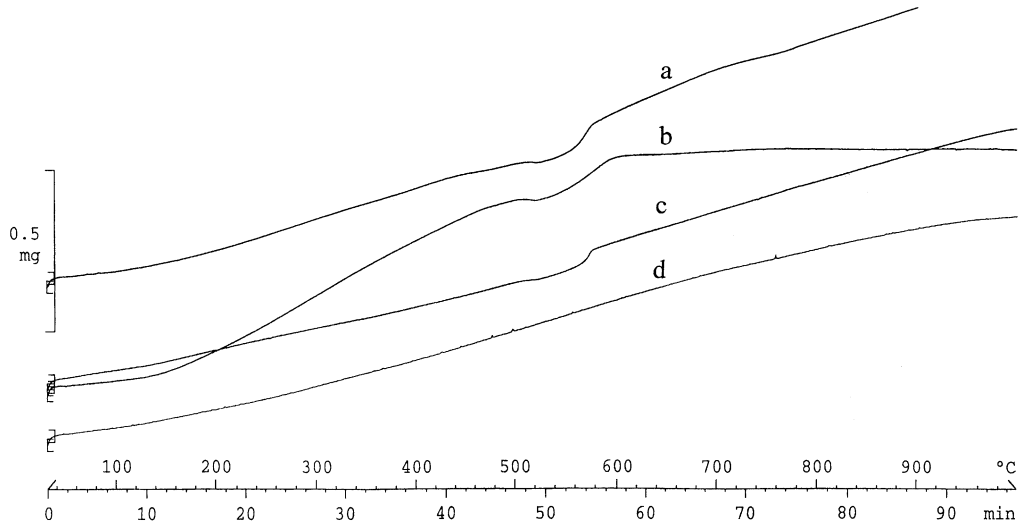

Fig. 5. TGA curves with and without a magnetic force measurement. (a), (b) and (c) were measured with a magnet; (d) was measured without magnet.

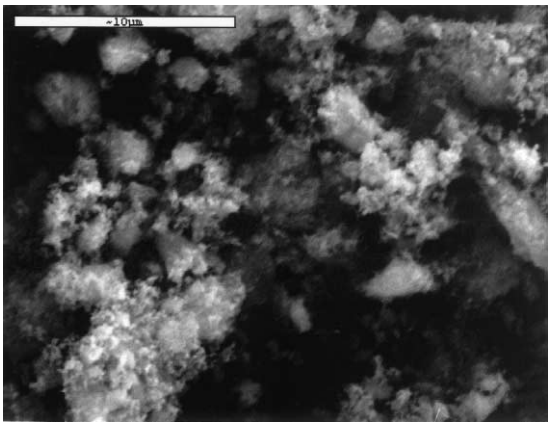

Fig. 6. An SEM image of the as-prepared sample.

Fig. 7a shows the same crystalline particles disperse in a spongelike material whose imaging density is very low. Combining the XRD and the DSC results leads to the conclusion that the well-shaped particles are silver nanocrystals and the sponge-like shapes are mixtures of amorphous Fe_2O_3 and amorphous Ag. Fig. 7b shows the as-prepared sample annealed under Ar at 350°C for 2 h. Based on the XRD results, the particles observed are a mixture of Ag and Fe_2O_3. Fig. 7c shows the reduced NC Fe/Ag sample, which is prepared under pure H_2 at 300°C for 1.5 h. Although some NC Fe/Ag particles are aggregated, the average size is still around 30 nm. The TEM results indicate that the NC Fe/Ag alloy is homogeneous.

3.4. Magnetization measurements

Fig. 8 is the room temperature magnetization loop of nanocrystalline Fe/Ag (70 : 30) after annealing the as-prepared Ag/Fe_2O_3 product under H_2 at 300°C. The curve shows that NC Fe/Ag has the typical ferromagnetic characteristics; the saturation magnetization, remanent magnetization, and coercivity field are 125 emu/g, 17.5 emu/g and 84 Gs, respectively. Considering that there is 0.55 g Fe in 1 g NC Fe/Ag if it has 70% Fe atoms and 30% Ag atoms, and that 1 g crystalline Fe has a 218 emu saturation magnetization moment at room temperature, 0.55 g crystalline Fe should have 120 emu magnetic moment under the intense applied field. Fig. 8 shows the NC Fe/Ag sample with the saturation magnetization 125 emu/g; it is in quantitative agreement with the saturation magnetization deduced from the atomic ratio of sample.

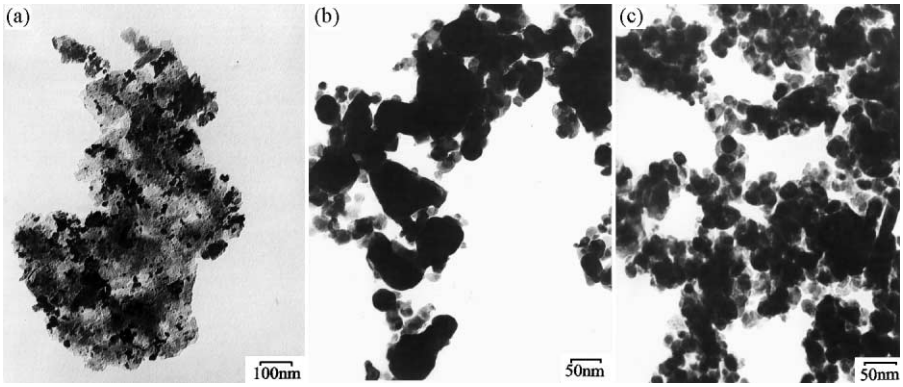

Fig. 7. The TEM images of the samples (Fe : Ag = 70 : 30). (a) The as-prepared sample; (b) the as-prepared sample, annealed under Ar at 350°C for 2 h; (c) the as-prepared sample, annealed under H_2 at 300°C for 1.5 h.

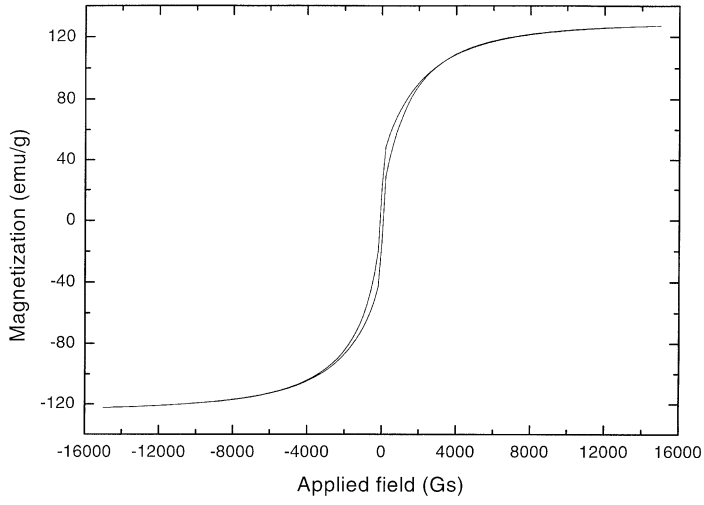

Fig. 8. Magnetization loop of nanocrystalline Fe/Ag (70 : 30) at room temperature.

In order to enable measurements of electrical resistivity and magnetoresistance of samples of Ag_xFe_{1-x}, the powders were first pressed in the form of solid pellets and then electrically wired for customary four point measurements. The as-prepared samples exhibited a semiconducting-like behavior. After thermal annealing at 723 K for 1 h in a gas mixture of 80% N_2 and 20% H_2, the samples became metallic. Magnetoresistance of annealed samples was measured at various temperatures. The results observed for $Ag_{0.50}Fe_{0.50}$ at 70 K are shown in Fig. 9. It should be noted that no special attempt was made to devise a composition of Ag/Fe for maximum MR. The purpose of this study was mainly to demonstrate that the negative magnetoresistance of the sonochemically synthesized powders is similar in nature to that found in granular metallic thin layers [30]. In both cases, the MR originates itself by a spin scattering mechanism. It is known that the highest MR values may be obtained for a lower concentration of nano-size ferromagnetic (Fe) particles [30].

Ferromagnetic resonance (FMR) measurements of powder samples were carried out using a Bruker EMX-220 digital X-band (9.40 GHz) spectrometer equipped with a Bruker ER 4121VT temperature

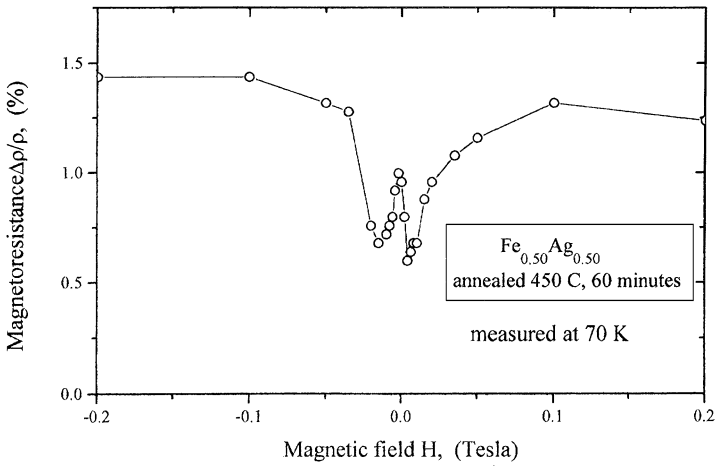

Fig. 9. Magnetoresistance of annealed $Ag_{0.46}Fe_{0.54}$ sample, measured at 77 K.

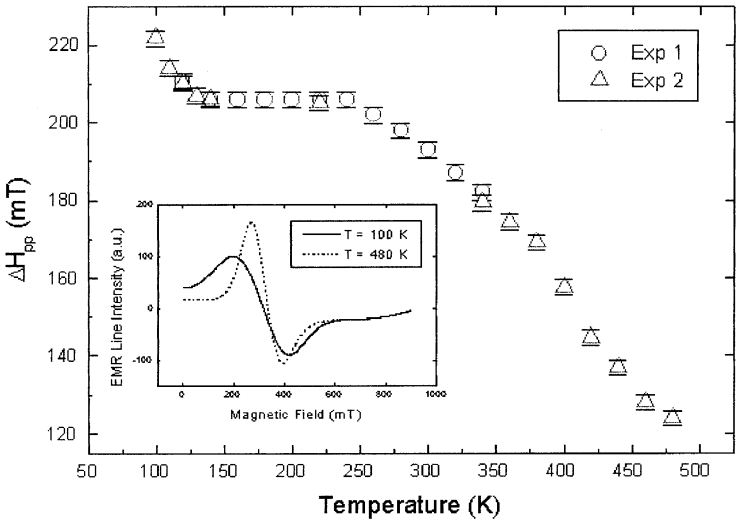

Fig. 10. Electron magnetic resonance (EMR) linewidth, ΔH_{pp} of annealed sample of $Ag_{0.46}Fe_{0.54}$ vs. T. The linewidth at the extreme temperatures of our measurements are shown in the inset.

controller for the $100 < T < 480$ K range. The spectral processing and calculations of the parameters were performed by Bruker's WIN-EPR software. In order to avoid size effects and cavity overloading, powder samples of several mg were placed at the bottom of a 1 mm glass capillary tube centered in the rectangular cavity. All measurements were performed in the linear response regime of microwave power of 200 mW. As expected, the FMR exhibits broad lines at low temperatures that become narrower as T approaches T_c. The linewidth ΔH_{pp} vs. temperature in the $100 < t < 480$ K range is shown in Fig. 10. The double integrated intensity of the resonance lines (DIN) is also presented in the same temperature range (see Fig. 11). The sharp decrease in DIN around 480 K may indicate that the major volume of the sample is ferromagnetic below this temperature. Above this temperature, a significant part of the Fe particles starts to exhibit super-

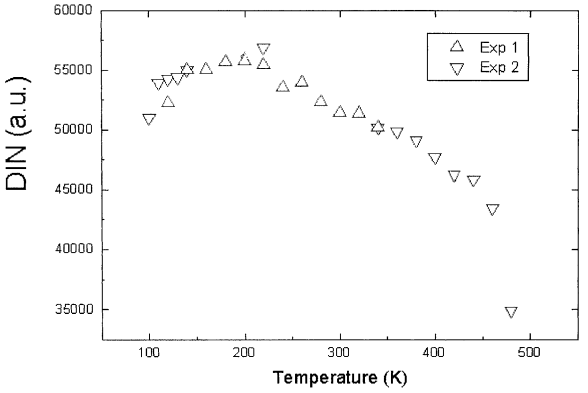

Fig. 11. Double integrated resonance signals vs. temperature.

paramagnetic behavior, which is consistent with the results observed for ΔH_{pp}.

The Mössbauer spectra measured at 85 and/or 300 K for the amorphous and crystalline Ag/Fe samples are displayed in Fig. 12. Two sub-spectra are observed (Fig. 12a) with a relative ratio of 7.4 : 1, corresponding to two equivalent Fe sites in the as-prepared amorphous material. The major sub-spectrum exhibits a broad doublet, which clearly indicates that no long range magnetic ordering is present. The hyperfine parameters of this doublet (at 85 K) are: IS = 0.27(1) and quadrupole splitting $\Delta = eqQ/2 = 1.10(1)$ mm/s, with a common linewidth of 0.75(1) mm/s. This doublet probably correspond to the non-magnetic amorphous Fe_2O_3 phase. In addition, the spectrum contains a minor broad sextet. The interpretation of the sextet yields: IS = 0.22(1) mm/s, and the hyperfine magnetic splitting of $H_{eff} = 505(2)$. The sextet does not show a quadrupole effect. The data obtained differ slightly from the measured magnetic hyperfine field values of γ-Fe_2O_3, which are: IS = 0.24 mm/s, $H_{eff} = 520(1)$ kOe, and an effective quadrupole splitting of $-0.20(1)$ mm/s [31].

Fig. 12b, shows the MS of Ag/Fe as-prepared material after annealing under Ar at 350°C for 1.5 h. The main information obtained from visual and computer analysis is the presence of two magnetic sextets with a relative ratio of 6 : 1. The hyperfine parameters of the intense sextet are exactly the same as the minor sextet in Fig. 12a.

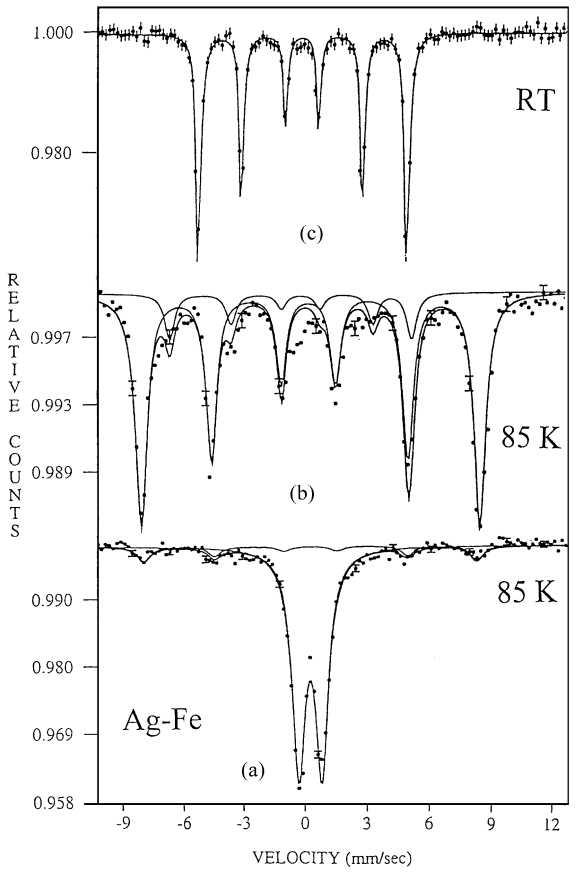

Fig. 12. Mössbauer spectra of the $Ag_{0.46}Fe_{0.54}$ samples: (a) the as-prepared amorphous sample, measured at 85 K; (b) the as-prepared sample annealed at 350°C under Ar, measured at 85 K; (c) the as-prepared sample reduced by H_2 a 300°C measured at 300 K.

Thus, the major part of the sample is the crystalline γ-Fe_2O_3 phase. The hyperfine parameters of minor sextet are: IS = $-0.45(1)$ mm/s, and $H_{eff} = 360(2)$. This sextet does not also show a quadrupole effect, and its origin has not yet been determined.

On the other hand, a single well-defined sextet (with IS = 0 and $\Delta = 0$) is obtained after annealing the sample under H_2 at 300°C for 1.5 h. The magnetic hyperfine field at ambient temperature, $H_{eff} = 336(2)$, indicates clearly the presence of pure Fe metal. Thus, annealing under hydrogen reduces γ-Fe_2O_3 into pure Fe metal.

3.5. Proposed mechanism for the NC Fe/Ag

The chemical reactions driven by intense ultrasonic waves strong enough to produce cavitation are oxidation, reduction, dissolution, and decomposition [32–36]. Here, the reaction system has two liquid phases: one is $Fe(CO)_5$, organic phase; the other is the aqueous phase $Ag(NH_3)_2^+$. It is well known that $Fe(CO)_5$ will be decomposed into amorphous Fe and CO under intense ultrasound in the organic phase [24]. On the other hand, there are three different regions formed during the aqueous sonochemical process [37–39]: (a) the inner environment (gas phase) of the collapsing bubble, where elevated temperatures (several thousands of degrees) and pressures (hundreds of atmospheres) are produced, causing water to vaporize and further pyrolyze into H and $OH^{\cdot}$ radicals; (b) the interfacial region, where the temperature is lower than in the gas-phase region, but still high enough to induce a sonochemical reaction; and (c) the bulk solution, which is at ambient temperatures and which is where the reaction between reactant molecules and $OH^{\cdot}$ or $H^{\cdot}$ takes place. Among these three regions, it appears that the sonochemical reaction occurs within the interfacial region, yielding amorphous materials, owing to the very high quenching rate experienced by the products.

The formation mechanism for the mixture of amorphous iron oxide and silver nanoparticles takes into consideration the radical species generated from water molecules by the absorption of ultrasound (Eq. (1))

$$H_2O \rightarrow H^{\cdot} + OH^{\cdot}. \quad (1)$$

A possible pathway for the formation of iron oxide, Fe_2O_3, could be the partial oxidation of Fe by secondary species formed by the recombination of H and OH radicals. In the absence of any additives or scavengers, H and OH radicals readily recombine to yield a variety of products, as shown in Eq. (2) [36].

$$2H^{\cdot}/2OH^{\cdot} \rightarrow H_2/H_2O_2/H_2O. \quad (2)$$

The oxidant H_2O_2 thus generated can initiate the oxidation of iron metallic clusters into iron oxide (Eq. (3)):

$$Fe^{\circ} + H_2O_2 \rightarrow Fe_2O_3 + H_2O. \quad (3)$$

At the same time, $Ag(NH_3)_2^+$ ions are reduced by partial initial iron into silver nanoparticles (Eq. (4)). We have to point out that we chose the complex, $Ag(NH_3)_2^+$, instead of $AgNO_3$, because the complex can slow down the reaction with $Fe(CO)_5$.

$$Ag(NH_3)_2^+ + FeFe^{2+} + Ag + 2NH_3. \quad (4)$$

Reactions (3) and (4) occur at the same time, resulting in the mixture of amorphous Fe_2O_3 and Ag nanoparticles, which are homogeneous.

In the post-reduction process, the homogeneous mixture is easy to reduce into a NC Fe/Ag system under pure H_2 at a relatively low temperature (300°C). Although the particles grow bigger, the average size is still around 30 nm.

4. Conclusion

Amorphous iron is obtained when $Fe(CO)_5$ is decomposed in an organic solvent. In an aqueous solution, Fe_2O_3 is obtained, and therefore in the process of preparing the Fe/Ag alloy, an additional step, the reduction of the oxide, is required. The TEM pictures show that while for the Ag/Fe_2O_3 mixture a nonhomogeneous material is obtained, the nanophased alloy Ag/Fe is completely homogeneous. It seems that while silver and iron are known not to disssolve on the nanoscale level, good miscibility is obtained.

References

[1] A. Henglein, Chem. Rev. (Washington, DC) 89 (1989) 1861.
[2] M. Greenblatt, Chem. Rev. 88 (1988) 31.
[3] S. Forster, M. Antonietti, Adv. Mater. 10 (1998) 195.
[4] M. Moffit, A. Eisenberg, Chem. Mater. 7 (1995) 1178.
[5] K. Ghosh, S.N. Maiti, J. Appl. Polym. Sci. 60 (1996) 323.
[6] R.P. Andres, J.D. Bielefeld, J.I. Henderson, D.B. Janes, V.R. Kolagunta, C.P. Kubiak, W.J. Mahoney, R.J. Osifchin, Science 273 (1996) 1960.
[7] B. Abeles, in: R. Wolfe (Ed.), Applied Solid State Science: Advances in Materials and Device Research, Academic Press, New York, 1976, p. 1.

[8] B. Abeles, P. Sheng, M.D. Counts, Y. Arie, Adv. Phys. 24 (1975) 407.
[9] C.I. Chen, Appl. Phys. 69 (1991) 5267.
[10] E.F. Kneller, J. Appl. Phys. 35 (1964) 2210.
[11] D. Korn, H. Pfeifle, Z. Phys. B 23 (1976) 23.
[12] F. Kajzar, G. Parette, J. Appl. Phys. 50 (1979) 1966.
[13] G. Longworth, R. Jain, J. Phys. F 8 (1978) 351.
[14] K. Sumiyama, N. Kataoka, Y. Nakamura, Jpn. J. Appl. Phys. 27 (1988) 1693.
[15] A. Crespo-Sosa, P. Schaaf, W. Bolse, K.-P. Lieb, M. Gimbel, U. Geyer, C. Tosello, Phys. Rev. B 53 (1996) 14795.
[16] K. Sumiyama, Y. Nakamura, Phys. Stat. Sol. (a) 81 (1984) K109.
[17] K. Sumiyama, T. Yoshitake, Y. Nakamura, Acta Metall. 33 (1985) 1785.
[18] N. Kataoka, K. Sumiyama, Y. Nakamura, J. Phys. F 15 (1985) 1405.
[19] Q.A. Pankhurst, N.S. Cohen, M. Odlyha, J. Phys.: Condens. Matter. 10 (1998) 1665.
[20] G. Mazzone, M.V. Antisari, Phys. Rev. B 54 (1996) 441.
[21] H.-M. Lin, C.-Y. Tung, Y.D. Yao, Y. Hwu, W.-L. Tsai, S.-J. Tzeng, C.-K. Lin, P.-Y. Lee, Nano Struct. Mater. 10 (1998) 457.
[22] K. Sumiyama, S.A. Makhlouf, S. Yamamuro, Y.-F. Xu, T.J. Konno, K. Wakoh, T. Hihara, K. Suzuki, J. Magn. Magn. Mater. 140–144 (1995) 563.
[23] C.L. Chien, J.Q. Xiao, J.S. Jiang, J. Appl. Phys. 73 (1993) 5309.
[24] K.S. Suslick, S.-B. Choe, A.A. Cichowlas, A.A. Grinstaff, Nature 353 (1991) 414.
[25] M.W. Grinstaff, M.B. Salamon, K.S. Suslick, Phys. Rev. B 48 (1993) 269.
[26] K.S. Suslick, M. Fang, T. Hyeon, A.A. Cichowlas, in: K.E. Gonsalves (Ed.), Molecularly Designed Nanostructured Materials, Materials Research Society, Pittsburgh, 1994.
[27] R. Bellissent, G. Galli, T. Hyeon, S. Magazu, D. Majolino, P. Migliardo, K.S. Suslick, Phys. Scr. T57 (1995) 79.
[28] K.V.P.M. Shafi, A. Gedanken, R.B. Goldfarb, I. Felner, J. Appl. Phys. 81 (1997) 6901.
[29] K.V.P.M. Shafi, A. Gedanken, R. Prozorov, J. Mater. Chem. 8 (1998) 769.
[30] N. Peleg, G. Gorodetsky, J. Magn. Mater. 191 (1998) 354.
[31] N.N. Greenwood, T.C. Gibb, Mossbauer Spectroscopy, Chapman & Hall Ltd. London, 1971, p. 251.
[32] K.S. Suslick (Ed.), Ultrasound: Its Chemical, Physical and Biological Effects, VCH, Weinheim, 1988.
[33] A.E. Alegria, Y. Lion, T. Kondo, P. Riesz, J. Phys. Chem. 93 (1989) 4908.
[34] M. Gutierrez, A. Henglein, J. Phys. Chem. 92 (1988) 2978.
[35] J.Z. Sostaric, P. Mulvaney, F. Grieser, J. Chem. Soc. Faraday Trans. 91 (1995) 2843.
[36] M. Gutierrez, A. Henglein, J. Dohrmann, J. Phys. Chem. 91 (1987) 6687.
[37] K.S. Suslick, D.A. Hammerton, IEEE Trans. Sonics Ultrason. SU-33 (1986) 143.
[38] K.S. Suslick, D.A. Hammerton, Ultrason. Int. (1985) 231.
[39] K.S. Suslick, R.E. Cline, D.A. Hammerton, Ultrason. Symp. Proc. 2 (1985) 1116.